Numerical Simulation Study of the Thermal Response Process of GAP Solid Propellant under Nozzle Structural Constraints

Junsen Yang, Hanqing Xia, Xingyuan Wang, Songlin Guo, Yi Wu
School of Aerospace Engineering, Beijing Institute of Technology
Beijing, China

1 Introduction

Solid propellants, which are enhanced composite energetic materials containing particles like AP, RDX, and others. The thermal response of high-energy propellants to thermal loading is a highly complex process, involving force-thermal-chemical coupling [1,2] and reactions that span multiple time and spatial scales, which significantly complicates both simulation and experimental observation. Early studies on the thermal response of high-energy propellants primarily focused on heat conduction and thermal decomposition, often overlooking the complex microscopic physical and chemical changes occurring within the propellant. With advancements in numerical methods, phase transitions and multi-component chemical reactions during thermal decomposition have been incorporated, allowing for more detailed analysis of temperature, pressure, and component concentration distributions during the process [3-4]. Furthermore, models have been developed to describe the microscopic pore expansion, gas permeation, and crack propagation in various energetic materials, providing accurate representations of their thermal response characteristics [5]. In simulating propellant cook-off conditions, simple structural constraints have been used in the design of cook-off devices to analyze how structural parameters affect the thermal response [6-7]. However, these models are primarily based on the thermal decomposition characteristics of the material itself, focusing mainly on the pre-ignition heat conduction process, and lack the quantitative descriptions of the full evolution from expansion and ignition to the combustion-to-detonation transition. Therefore, this study employs a two-dimensional transient numerical model, based on chemical reaction kinetics and multiphase flow phase-change coupling processes, to investigate the transient combustion-to-detonation transition under thermal stimuli in solid rocket engines.

2 Experiments setup

To simulate the ignition response behavior of the propellant under the structural constraints of the engine, a test specimen was designed featuring a combustion chamber structure with propellant, as well as an engine nozzle. As shown in Figure 1, the entire experimental system consists of four components: the engine structural test specimen, a temperature control system, a high-speed shadowgraph diagnostic system, and a pressure-temperature acquisition system.

Correspondence to: yi.wu@bit.edu.cn

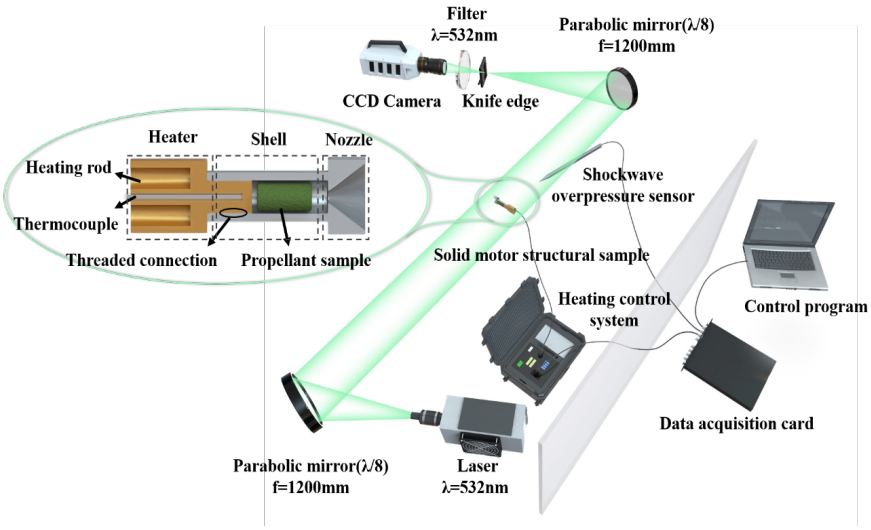

Figure 1: Schematic of the experimental setup

The motor structural test piece, as shown on the left side of Figure 1, is primarily made of aluminum alloy. A heating component is located on the left side of the aluminum structure, with a temperature control system utilizing an electric heating rod, allowing for controllable heating rates. A K-type thermocouple (TT-K-30-SLE) is used to monitor the temperature of the heated test piece shell. To enable quantitative assessment of thermal stimulation response intensity, a shock wave overpressure sensor (SCYG312) is placed 30 cm away from the test piece to measure the overpressure of shock waves generated after the ignition of the propellant sample. A Z-type high-speed schlieren imaging system was utilized to record the cook-off response process of the motor test piece. The sample is placed between two concave mirrors with a focal length of 1200 mm. The high-speed camera employed is the Revealer X213, configured with a frame rate of 50,000 fps and an exposure time of 0.1 μs.

The propellant samples selected are composed of the main components: 27% by mass GAP binder, 10% by mass RDX, 45% by mass ammonium perchlorate (AP) oxidizer, and 18% by mass aluminum particles. The propellant specimens were processed into cylindrical samples measuring ϕ10 × 20 mm, with a mass of 11.3 g, and were placed within the motor structural constraint test piece.

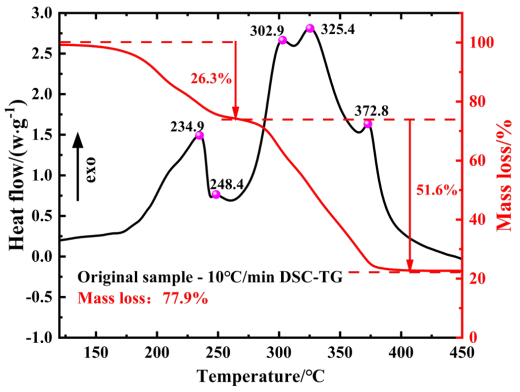

Figure 2: TG and DSC Curves of GAP Propellant under Atmospheric Pressure in a Nitrogen Environment

To obtain the thermal decomposition chemical reaction kinetics parameters of the propellant, a Netzsch STA 449F5 simultaneous thermal analyzer was used to investigate the thermal decomposition kinetics

characteristics of the GAP propellant via differential scanning calorimetry (DSC), which is shown in Figure 2. The experimental conditions were set in a nitrogen atmosphere (purity greater than 99.99%) with a flow rate of 20 ml/min and heating rates of 10 °C/min over a temperature range of 20–450 °C.

3 Simulation method

To investigate the detonation mechanism of GAP-based solid propellants under slow thermal stimulation, a thermal response model for a solid rocket motor was developed based on chemical reaction kinetics. The model replicates the experimental geometry, as shown in Figure 3, and includes the casing region, propellant sample region, nozzle region, and far-field region. The model employs a structured mesh with a grid thickness of 0.1 mm. The mesh in the boundary layer is refined with the first mesh height of 0.001 mm to ensure y+ $\leqslant$ 1. The heater component of the structural test specimen was simplified in the model, retaining only the end face as the thermal load application surface. The applied heat flux density was 3.8 W·m^{-2}.

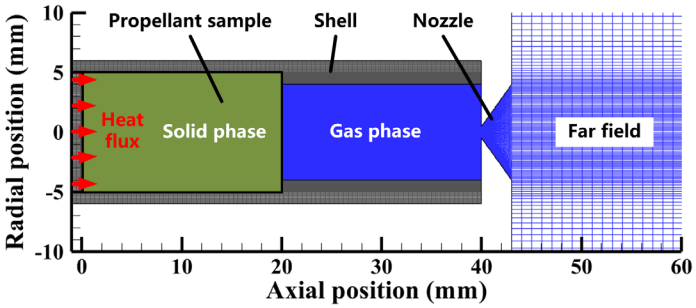

Figure 3: Computational region meshes of the solid rocket

Considering the heat dissipation characteristics of stainless steel, the solid wall surface was modeled as a no-slip, heat-transfer boundary with a fixed temperature of 300 K. The thermal conductivity of stainless steel was specified as 16.27 W/(m·K), and its specific heat capacity was 502.48 J/(kg·K).The outlet boundary condition was defined as a pressure far-field boundary with P = 1atm and T = 300 K.

Considering the axisymmetric geometry of the solid rocket, a two-dimensional axisymmetric unsteady Navier–Stokes equation comprising continuity, momentum, energy, and species has the following form:

$$\frac{\partial U}{\partial t}+\frac{\partial (F_x-G_x)}{\partial x}+\frac{\partial (F_r-G_r)}{\partial r}=S \qquad \text{(Eq.1)}$$

Where,

$$U=\begin{bmatrix}\rho_i\\ \rho v_x\\ \rho v_r\\ \rho E\\ \rho Y_i\end{bmatrix},\quad F_x=\begin{bmatrix}\rho_i v_x\\ \rho {v_x}^2+P\\ \rho v_x v_r\\ v_x(\rho E+P)\\ \rho Y_i v_x\end{bmatrix},\quad F_r=\begin{bmatrix}\rho_i v_r\\ \rho v_x v_r\\ \rho {v_r}^2+P\\ v_r(\rho E+P)\\ \rho Y_i v_r\end{bmatrix},\quad S=\begin{bmatrix}S_m\\ S_{v_x}\\ S_{v_r}+\frac{P-\tau_s}{r}\\ S_e\\ S_Y\end{bmatrix},$$

$$G_x=\begin{bmatrix}0\\ \tau_{xx}\\ \tau_{xr}\\ k\frac{\partial T}{\partial x}+\rho\sum_i h_i J_{i,x}+u\tau_{xx}+v\tau_{xr}\\ -J_{i,x}\end{bmatrix},\quad G_r=\begin{bmatrix}0\\ \tau_{rx}\\ \tau_{rr}\\ k\frac{\partial T}{\partial r}+\rho\sum_i h_i J_{i,r}+u\tau_{rx}+v_r\tau_{rr}\\ -J_{i,r}\end{bmatrix},$$

Vx and Vr are the axial and radial velocities, respectively. Y is the mass fraction of species, P is the pressure, $k\frac{\partial T}{\partial r}$ is the heat conduction flux, h and J are the diffusion flux and sensible enthalpy for species, respectively, and τ is the viscous stress. S contains mass, momentum, energy, and species source terms related to chemical reactions and gas-solid phase transition.

On the basis of the Boussinesq hypothesis, the realizable k–ε turbulent model was used in this study. The transport equations for the kinetic energy and turbulence eddy are given as follows:

$$\frac{\partial}{\partial t}(\rho k)+\frac{\partial}{\partial x}(\rho v_x k)+\frac{1}{r}\frac{\partial}{\partial r}(r\rho k v_r)=\frac{\partial}{\partial x}\left(\alpha_k\mu_{eff}\frac{\partial k}{\partial x}\right)+\frac{1}{r}\frac{\partial}{\partial r}\left(r\alpha_k\mu_{eff}\frac{\partial k}{\partial r}\right)+G_k-\rho\varepsilon \quad \text{(Eq.2)}$$

$$\frac{\partial}{\partial t}(\rho\varepsilon)+\frac{\partial}{\partial x}(\rho\varepsilon v_x)+\frac{1}{r}\frac{\partial}{\partial r}(r\rho\varepsilon v_r)=\frac{\partial}{\partial x}\left(\alpha_\varepsilon\mu_{eff}\frac{\partial\varepsilon}{\partial x}\right)+\frac{1}{r}\frac{\partial}{\partial r}\left(r\alpha_\varepsilon\mu_{eff}\frac{\partial\varepsilon}{\partial r}\right)+C_{1\varepsilon}\frac{\varepsilon}{k}G_k- \quad \text{(Eq.3)}$$
$$C_{2\varepsilon}\frac{\varepsilon^2}{k}\rho-R_\varepsilon$$

where the quantities α_ε and α_k are the inverse effective Prandtl numbers for k and ε. The constants $C_{1\varepsilon}$, $C_{2\varepsilon}$, and C_μ are set at 1.44, 1.92, and 0.09, respectively.

Table 1: Components of the pyrolysis products

Pyrolysis product	C_4H_6	C_2H_4	Al	O_2	NH_3	HCl	N_2	Other
Proportion (%)	7.3	5.7	18	30	7.5	16.2	15.2	<0.1%

Table 2: Components of the combustion products

Combustion product	N_2	CO_2	H_2O	CO	O_2	Al_2O_3	Cl_2	Other
Proportion (%)	85.80	12.97	1.43	1.09	0.26	0.58	0.36	<1%

According to the primary combustion characteristics of gap propellent, the combustion mode includes oxidative combustion and anoxic pyrolysis. To evaluate the main chemical reactions in these two processes, the combustion process of the solid fuel was analyzed via chemical equilibrium analysis (CEA) software. The components of the pyrolysis and combustion products are listed in Table 1 and Table 2.

Subsequently, the combustion products of GAP propellant in an air environment, including N_2, CO_2 , H_2O , O_2 , CO, and Al_2O_3, were identified. To simulate the combustion reactions of the GAP propellant, a 12-species, 5-step chemical reaction mechanism was employed, as detailed in Table 3.

Table 3: Chemical reaction mechanism

No.	Reaction Model	A (s^{-1})	E/R (K)
1	$C_2H_4 + O_2 \rightarrow 2\ CO + 2\ H_2O$	1.125E10	15107
2	$C_4H_6 + 3.5\ O_2 \rightarrow 4\ CO + 3\ H_2O$	8.8E11	15200
3	$CO + 0.5\ O_2 \rightarrow CO_2$	3E12	25000
4	$2\ Al + 1.5\ O_2 \rightarrow Al_2O_3$	9.7E13	9600
5	$2\ NH_4ClO_3 \rightarrow N_2+H_2O+Cl_2+ 2\ O_2$	1E8	11060

In addition to the pyrolysis of the solid propellant and the combustion of gas-phase pyrolysis products, the heat release from the combustion of the high-energy solid propellant itself is also significant and cannot be overlooked. For the ignition and combustion process of the solid propellant, a pressure-dependent ignition growth model is typically used to describe the reaction rate of the solid-phase combustion:

$$\frac{\mathrm{d}Y}{\mathrm{d}t} = G_1(1-Y)^c P^y \qquad \text{(Eq.4)}$$

Here, Y represents the mass fraction of the GAP propellant, t is time, and P is the combustion pressure. For the given propellant, G_1, c and y are constants, with values set to 400, 0.67, and 2, respectively.

Given that the GAP propellant exhibits characteristics similar to a viscous fluid under heated conditions, it is approximated as an incompressible viscous fluid to represent its physical properties, with a density of 1884 kg/m³. Additionally, the ideal gas assumption is applied to all gas-phase fluids. The mixture properties are defined as the mass-weighted average of the individual component parameters.

The governing equations are the two-dimensional Reynolds-averaged Naiver–Stokes equations for the gas phase, and a pressure-based finite volume solver is employed to solve the unsteady Naiver–Stokes equations. The pressure implicit with splitting of operators (PISO) solver is used to construct numerical upwind fluxes, and a third-order monotonic upstream-centered scheme for conservation laws (MUSCL) scheme is employed to solve the species transport equations. A bounded second-order implicit scheme is used for time integration. To ensure numerical stability, the Courant–Friedrichs–Lewy (CFL) number is maintained below 0.5, corresponding to time step sizes on the order of 10^{-5} seconds.

4 Model validation against experiments

To validate the developed model, Figure 4 compares the local temperature rise and external flow field changes of the GAP propellant under thermal loading, as obtained from both experimental and simulation results.

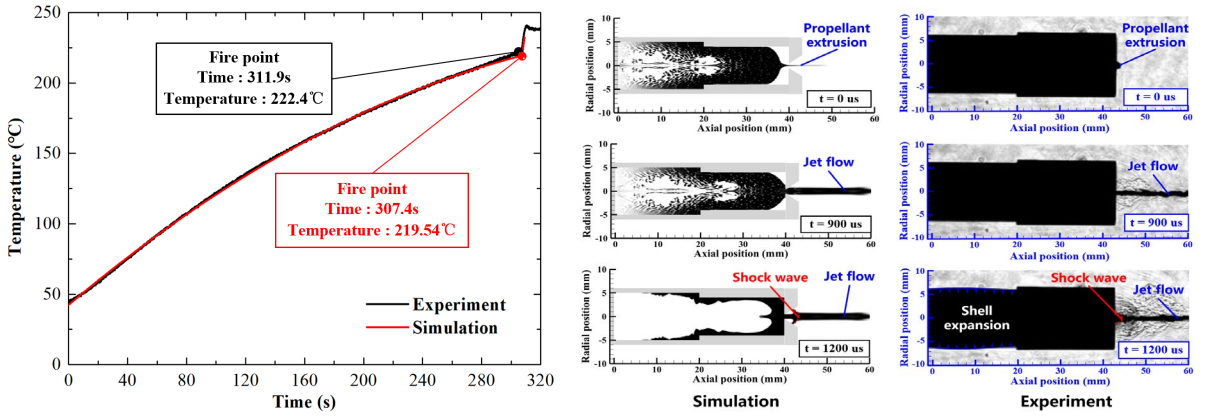

Figure 4：Comparison of characteristic parameters in experimental measurement and numerical prediction: (A) the temperature at measurement points, (B) the flow structure out of solid rocket

The geometry and flow parameters in the simulation were identical to those used in the experiment. Given that the shadowgraph system primarily captures density variations within the flow field, Figure 4(B) compares the transient changes in flow field density. The results indicate that the simulation model effectively captures the entire process of engine heating and detonation.

Table 4 presents a comparison of the ignition and detonation characteristics of the propellant. The maximum deviation between the measured ignition delay time and the temperature at the measurement points is less than 2%, while the peak shockwave overpressure differs from the experimental results by approximately 0.7%. These comparisons provide a sufficient level of confidence in the thermal response model of the propellant.

Table 4: Comparison of transient characteristic parameters

Parameter	Experiment	Simulation	Error
Ignition time (s)	311.9	307.4	1.4%
Temperature of measure point (℃)	222.4	219.54	1.3%
Overpressure of shock wave (MPa)	0.153	0.152	0.7%

5 Conclusions

Based on the coupling process of chemical reaction kinetics and multiphase flow phase transitions, a two-dimensional transient numerical model was developed to study the transient combustion-to-detonation transition process under thermal loading in solid rocket engines. High-speed shadowgraphy was employed to capture the cook off response of the solid rocket, providing experimental validation for the developed model. The experimental results show a high degree of consistency with the simulation results, with the maximum deviation remaining under 2%.

References

[1] W. Chen, S. Wu, et al. Numerical simulation of the deflagration to detonation transition behavior in explosives based on the material point method. Combustion and Flame, 2022. 238.

[2] R. Gupta, M. Kumar, et al. Deflagration to Detonation Transition in Cast Explosives: Revisiting the Classical Model. Propellants, Explosives, Pyrotechnics, 2022. 47(3).

[3] P. Gillard, B. Longuet. Investigation of heat transfer and heterogeneous reactions during the slow cook off of a composite propellant. Journal of Loss Prevention in the Process Industries, 2013. 26(6): p. 1506-1514.

[4] M.L. Gross, K.V. Meredith, M.W. Beckstead. Fast cook-off modeling of HMX. Combustion and Flame, 2015. 162(9): p. 3307-3315.

[5] M.L. Hobbs, M.J. Kaneshige, et al. Cookoff modeling of a melt cast explosive (Comp-B). Combustion and Flame, 2020. 215: p. 36-50.

[6] W.W. Erikson, M.A. Cooper, et al. Determination of thermal diffusivity, conductivity, and energy release from the internal temperature profiles of energetic materials. International Journal of Heat and Mass Transfer, 2014. 79: p. 676-688.

[7] H. Işık, F. Göktaş. Cook-off analysis of a propellant in a 7.62 mm barrel by experimental and numerical methods. Applied Thermal Motorering, 2017. 112: p. 484-496.